Bifunctional Localized High-Concentration Electrolyte for the Fast Kinetics of Lithium Batteries at Low Temperatures

Pengbin Lai, Xiaodie Deng, Yaqi Zhang, Jialin Li, Haiming Hua, Boyang Huang, Peng Zhang,* and Jinbao Zhao*

Read Online

ACCESS | Metrics & More | Article Recommendations | Supporting Information

ABSTRACT: Traditional lithium batteries cannot work well at low temperatures due to the sluggish desolvation process, which limits their applications in low-temperature fields. Among various previously reported approaches, solvation regulation of electrolytes is of great importance to overcome this obstacle. In this work, a tetrahydrofuran (THF)-based localized high-concentration electrolyte is reported, which possesses the advantages of a unique solvation structure and improved mobility, enabling a Li/lithium manganate (LMO) battery to cycle stably at room temperature (retains 85.9% after 300 cycles) and to work at a high rate (retains 69.0% at a 10C rate). Apart from that, this electrolyte demonstrates superior low-temperature performance, delivering over 70% capacity at −70 °C and maintaining 72.5 mAh g^{-1} (≈77.1%) capacity for 200 cycles at a 1C rate at −40 °C. Also, even when the rate increases to 5C, the battery could still operate well at −40 °C. This work demonstrates that solvation regulation has a significant impact on the kinetics of cells at low temperatures and provides a design method for future electrolyte design.

KEYWORDS: localized high-concentration electrolyte, tetrahydrofuran, fast kinetics, solvation structure, low temperature
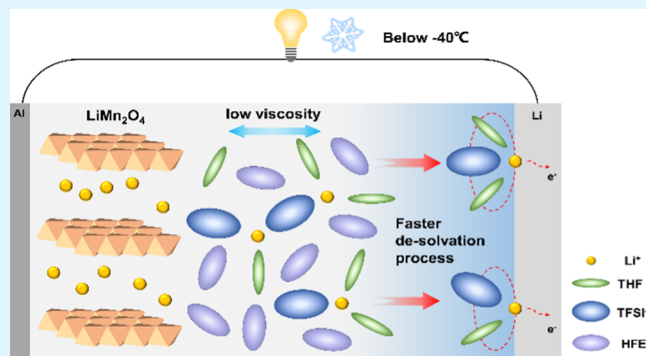
1. INTRODUCTION

Traditional lithium-ion batteries (LIBs) suffered significant capacity decay at a sub-zero environment, which restricted its applications in electric vehicle, polar exploration, aerospace, and so on.[1−5] To increase energy at low temperatures, replacing the graphite anode with lithium metal (3860 mAh g^{-1} theoretical capacity and −3.04 V vs the standard hydrogen electrode) is a promising step to push the battery's energy density to a higher level.[6] What is more, it has been reported that the stripping−plating mechanism of lithium metal showed better kinetics than a graphite anode, whose intercalation mechanism was regarded as the rate-determining step of LIBs at sub-zero temperature.[7]

Although they possess these merits, lithium metal batteries (LMBs) were notorious for their reaction with electrolytes and large volume changes during cycling. These properties resulted in low Coulombic efficiency (CE), limiting their practical applications. When the temperature decreased below −30 °C, LMBs also suffer from capacity decay and voltage drop.[8,9] This phenomenon can be ascribed to the following reasons including slower Li$^+$ transportation in bulk electrolytes and slower Li$^+$ diffusion through the solid-electrolyte interphase (SEI).[10−14] Generally speaking, slower Li$^+$ transportation at low temperatures can be mitigated by adding low-melting-

point solvents as co-solvents. The candidate solvents are ester,[15,16] ether,[17,18] nitrile,[19] sulfite,[20] and so on.

In recent works, it is believed that the sluggish Li$^+$ desolvation process was to blame for the poor low-temperature performance of the battery, which is related to the binding behavior of lithium ions with solvents or anions.[21,22] Previous literature[23] has confirmed the advantage of Li$^+$/anion binding in improving the low-temperature performance of lithium metal anodes. Therefore, by the above analysis, an ideal low-temperature electrolyte for LMBs with fast kinetics should satisfy the following criteria: (1) stable with lithium metal anodes, (2) low viscosity and high conductivity at low temperatures, and (3) containing an anion-dominant solvation structure. Recently, many efforts have been made on designing suitable electrolytes to adjust the solvation behavior of Li$^+$ to promote the desolvation process. One way is to select a solvent with a lower solvating ability with Li$^+$. Fan et al[24] developed an all-fluorinated electrolyte with a low binding ability with Li$^+$,
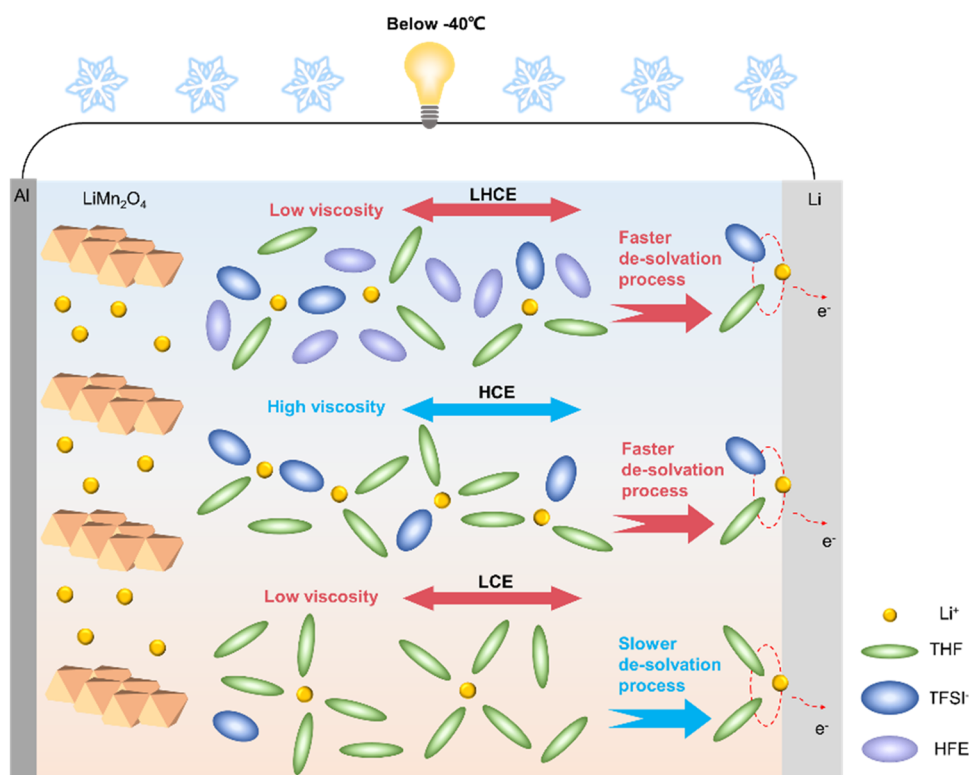
Figure 1. Schematic illustration of the lithium ion's transportation in different kinds of electrolytes.

enabling the Li/NCA cell to work at a wide temperature range (from −95 to 125 °C). Recently, there have been many molecular engineering strategies applied to reduce the binding ability with Li^{+} to improve the cell's low-temperature performance.[25−28]

Apart from that, another strategy, the localized high-concentration electrolyte (LHCE), seemed to be a better solution to the low temperature problem. The anion-containing solvation structure in the LHCE is regarded to be beneficial for the charge transfer process.[29] Also, the low viscosity of the LHCE facilitates the diffusion of Li^{+} in the bulk electrolyte, especially at low temperatures. Xia et al.[30] added dichloromethane (DCM) into the ethyl acetate (EA)-based high-concentration electrolyte (HCE), which reduced the viscosity of the electrolyte and made the battery work at −70 °C. Holoubek et al.[29] demonstrated a DME-based LHCE that enabled the full cell (N/P ratio is 2) to cycle at −40 °C. In addition, our previous work[31] reported a methyl propionate-(MP)/FEC-based LHCE, which enabled the 4.5 V Li/LCO cells to work at −70 °C.

In this work, a localized high-concentration tetrahydrofuran (THF)-based electrolyte is reported. THF is chosen as the basic solvent for its lower viscosity (0.53 cP), lower melting point (−108 °C), and higher solubility to lithium bis-(trifluoromethanesulphonyl)imide (LiTFSI).[32] This high-concentration electrolyte (HCE, concentration > 3 M) not only possesses a high oxidative potential, making them applicable in the 4V-class cell but also has a higher anion proportion in the solvation structure, which could facilitate the charge transfer process. To further improve the performance at low temperatures, the diluent 1,1,2,2-tetrafluoroethyl-2,2,3,3-tetrafluoro-propylether (HFE) was selected and added into the HCE, forming an LHCE. The introduction of HFE not only reduces the viscosity of the HCE by breaking the 3D network of the

HCE but also maintains the solvation structure of the HCE due to the weak binding ability of HFE with lithium ions. This LHCE combined the better mobility of low concentration and the unique solvation behavior of high concentration, which is beneficial for the application in the low-temperature field (Figure 1). With the optimized 5m-HFE41 electrolyte, the Li/LMO cells could cycle stably at room temperature and exhibit better high-rate performance. Apart from that, the cells in this electrolyte maintain 72.5 mAh g^{−1} (≈77.1%) capacity for 200 cycles at 1C and −40 °C. To our surprise, it could still work when we raised the rate to 5C, demonstrating excellent high-rate performance at low temperatures. This work shows the application of the LHCE strategy in the field of low temperatures. And we believe that this sort of strategy can provide a reference for the future design of low-temperature electrolytes.

2. EXPERIMENTAL SECTION

2.1. Computational Details. The density functional theory (DFT) calculation was run on the Gaussian09 package,[33] using the B3LYP-D3 method[34,35] at the 6-311+G(d,p) basis set.[36,37] In the MD simulation, an amorphous cell was packed with LiTFSI, THF, and HFE with a certain ratio. The cell was first geometry-optimized with the COMPASS (Condensed-Phase Optimized Molecular Potentials for Atomistic Simulation Studies) force field[38] (Figure S3). The Ewald summation[39] was used to calculate the long-range electrostatic interaction, and the van der Waals interaction was truncated at 18.5 Å. The relevant description can be seen in our previous work.[40] After that, another MD simulation with an NVT (constant volume and constant temperature) ensemble at different temperatures (298.15 K for room temperature) was conducted to investigate the diffusion of lithium ions in the bulk electrolyte. The diffusion coefficient is determined as follows
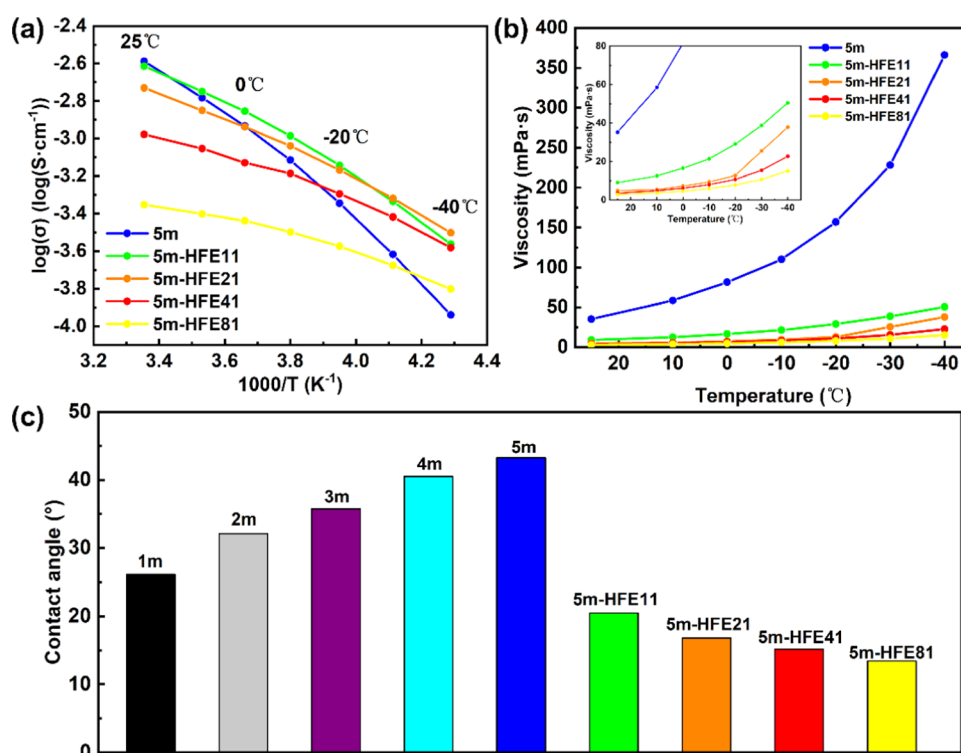
Figure 2. (a) Conductivity of electrolytes at different temperatures, (b) the viscosity of electrolytes at different temperatures, and (c) the values of the contact angle with the separator.

$$D = \frac{1}{6N_a} \lim_{t \to \infty} \frac{d}{dt} \sum_{i=1}^{N_a} \langle [r_i(t) - r_i(0)]^2 \rangle = \frac{1}{6} \lim_{t \to \infty} \frac{d}{dt} MSD \tag{1}$$

where N_a means the atom number and $r_i(t)$ and $r_i(0)$ represent the position of atom i at time t and 0, respectively.

2.2. Preparation of Materials. The cathode was prepared by mixing the lithium manganate (LMO) active material (Beijing Easpring Material Technology Co. Ltd), acetylene black, and poly(vinylidene fluoride) (PVDF) binder (8:1:1). *N*-Methyl-2-pyrrolidone (NMP) was added to disperse the agent. The cathode has a diameter of 12 mm and a mass loading of 3 mg cm^{-2}. For the anode, the thickness of lithium metal was 200 μm. The Celgard 2500 separator was purchased from the manufacturer.

The THF solvent (>99.5%) was obtained from Energy Chemical. The electrolyte was made by mixing the LiTFSI salt and THF solvent in specified molarities. The amount of diluent HFE in the 5m electrolyte was determined by the specific mass ratio. For instance, the 5m-HFE41 electrolyte was prepared by adding HFE into the 5m electrolyte in a mass ratio of 4:1.

2.3. Material Characterization. The conductivity was tested by a CHI660D electrochemical workstation. The viscosity value was obtained by a viscometer (VM-10A-L). The contact angle test was conducted by a JC-2000C1 tester. The X-ray diffraction (XRD) test angle ranged from 10 to 80° (Rigaku miniflex 600 X-ray diffractometer). Scanning electron microscopy (SEM) was conducted to analyze the morphology of the surface of the cathode and anode (Gemini SEM 500 field emission scanning electron microscope). X-ray photoelectron spectroscopy (XPS) spectra were obtained to analyze the element at the surface of the cathode and anode (Escalab Xi+ equipment). The electrode sample of SEM and XPS was obtained from dissembled cells and then rinsed with the THF solvent in a glovebox. The laser of the Raman test was 532 nm (HORIBA FRANCE). ^{7}Li NMR data was obtained by an Ascend 500 MHz spectrometer.

2.4. Electrochemical Characterization. Li/Li symmetry cells were applied to the Tafel test at a speed of 1 mV s^{-1}. The frequency of electrochemical impedance spectroscopy (EIS) characterization was from 10^{-1} to 10^5 Hz and the amplitude of voltage was 5 mV. The Li/LMO cells for the EIS test were in a fully discharged state. The average Coulombic efficiency (CE) of Li/Cu cells in electrolytes was determined using a modified Adam method 3.[41] All of the Li/LMO cells were CR-2016 type with 70 μL of electrolyte. The charge/discharge behavior of cells was tested on the Neware system. The battery was charged and discharged for one cycle at 0.1C to activate the battery. The low-temperature environment was provided by a DC-8006 incubator and a Meiling Biology & Medical DW-HW50 ultralow freezer. The activated cells were placed in the low-temperature environment for at least 2 hours to reach thermal equilibrium. The Li$^+$ transference number was measured in Li/Li symmetrical batteries in 2032-type coin cells, which was calculated by the following equation:

$$t_{Li^+} = \frac{I_s(\Delta V - I_i R_i)}{I_i(\Delta V - I_s R_s)}$$

in which ΔV is the applied voltage of 10 mV, I_i and I_s are the current at initial and steady states, respectively, and R_i and R_s are the corresponding impedances of the cell, respectively.

3. RESULTS AND DISCUSSION

The physical property of electrolytes is displayed in Figure 2. In Figure S2a, the conductivity of all electrolytes was decreased with the increase of salt concentration. The only exception is that the conductivity of 2m concentration is higher than 1m before −20 °C, which may be ascribed to the unsaturation of lithium salt at 1m concentration. When the temperature gradually decreased, electrolytes with various concentrations all showed a declining tendency. And it can be found that the higher the concentration, the more obvious the decrease. When introducing different amounts of diluent HFE into the 5m electrolyte, the conductivity is shown in Figure 2a. The conductivity of these electrolytes was lower than that of the 5m electrolyte at room temperature, which resulted from the low permittivity of HFE. However, the conductivity was higher
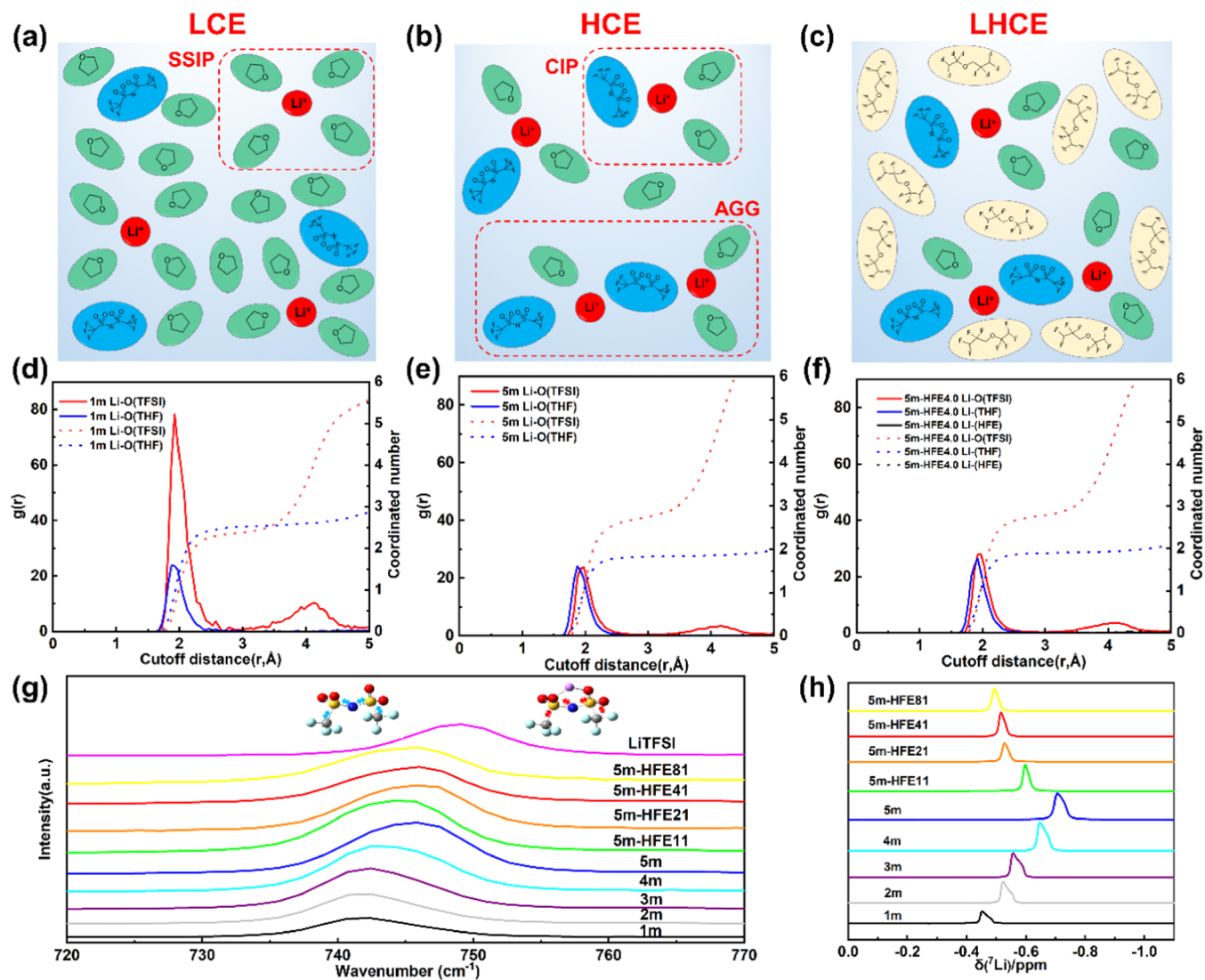
Figure 3. Result of the MD simulation of the three kinds of electrolytes and the simulation snapshot. (a-c) Schematic description of the solvation structure. (d−f) MD simulation result of three electrolytes. (g) Raman spectra of electrolytes. (h) ^7Li NMR comparison results.

than that of the 5m electrolyte, in turn, at −40 °C. This phenomenon indicates that the addition of HFE could inhibit the sharp decrease of conductivity of high-concentration electrolytes at low temperatures, demonstrating its viability in the low-temperature field (this is further discussed in Figure S1). And the viscosity of these electrolytes is shown in Figure S1b; the viscosity increases exponentially with the decrease of temperature, and the variation will become more obvious at higher concentrations (at −40 °C, the viscosity of 1m was 4.06 mPa·s, while that of 5m was 366 mPa·s). Such a high viscosity can be remarkably decreased by adding HFE. At −40 °C, the viscosity of 5m-HFE11, 5m-HFE21, 5m-HFE41, and 5m-HFE81 was 50.5, 37.8, 22.7, and 15.1 mPa·s, respectively. Meanwhile, the contact angle with the separator decreased from 43.3 (5m) to 20.5, 16.8, 15.2, and 13.4°, indicating the improvement of wettability (Figures 2c and S2). By comparing the above physical properties of these electrolytes, 5m-HFE41 was selected as the optimized electrolyte for the following tests.

To investigate the impact of salt concentration on the solvation structure, molecular dynamics (MD) and spectral analyses were conducted. The force field type of each atom and snapshots of various electrolytes are displayed in Figures S3

and S4, respectively. At low concentrations, the main solvation component around the lithium ion was the solvent and solvent-separated ion-pair (SSIP) structure. When the concentration was increased to 5m, a large proportion of THF molecules coordinated with lithium ions and the free THF solvent molecule was reduced. Meanwhile, the degree of association between lithium ions and anions will also be enhanced by the formation of a contact-ion pair (CIP) or an aggregate (AGG).[42] As the previous literature reported,[43] in the high-concentration electrolyte, there is an enhanced three-dimensional solvation network that suppresses the diffusion of lithium ions. When adding the diluent to the high-concentration electrolyte, due to the low binding ability with lithium ions, the diluent solvent did not enter the inner solvation layer and was distributed in the outer layer. As a result, the inner solvation layer of lithium ions is still a solvent structure dominated by the CIP or AGG as a high-concentration electrolyte, while the outer three-dimensional network was broken due to the introduction of diluents, which could facilitate the diffusion of lithium ions. The schematic illustration of the low-concentration electrolyte (LCE), HCE, and LHCE is displayed in Figure 3a−c, respectively.
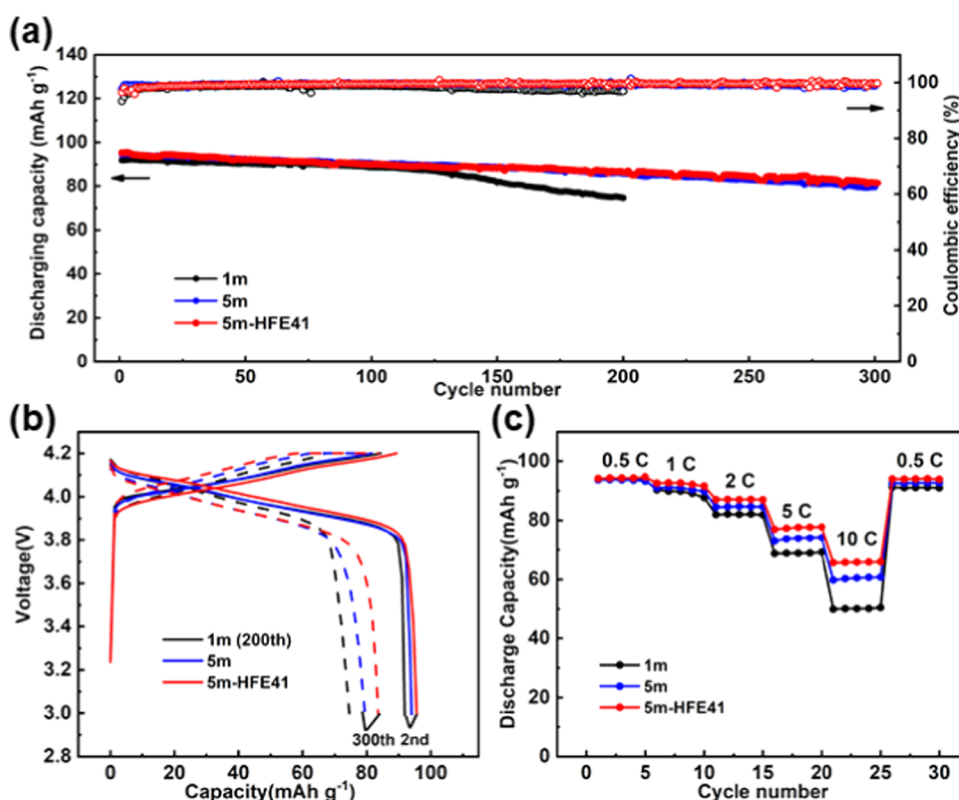
Figure 4. Electrochemical performance of Li/LMO cells. (a) Cycling performance at 1C and 25 °C. (b) Voltage-specific capacity curve for the specified cycle of three electrolytes. (c) Rate performance.

The MD simulation result of the three kinds of electrolytes is shown in Figure 3d−f. The coordination number (CN) was increased from 2.2 of the 1m electrolyte to 2.7 of the 5m electrolyte. On the other hand, the CN of THF with Li+ decreased from 2.4 to 1.7. (Table S1) In a comprehensive comparison, the proportion of Li+ with anion association (CIP or AGG) increased, while the proportion of SSIP decreased. In addition, in the 5m-HFE41 electrolyte, the CN of lithium ions with the anion and THF solvent was 2.6 and 1.7, respectively, which is nearly the same as that for the 5m electrolyte. The MD result indicated that the inner solvated structure of the high-concentration electrolyte was not significantly changed with the introduction of HFE. The MD result of other electrolytes is shown in Figure S5.

The result of theoretical calculations could be confirmed by the spectral analysis. In Figure 3g, the peak at around 750 cm^{-1} represents the S−N vibration of LiTFSI.[44] The peak gradually approached pure LiTFSI (748.9 cm^{-1}) from 1m (742.2 cm^{-1}) to 5m (745.2 cm^{-1}), indicating the strengthening of the vibration and more Li+ paired with the TFSI$^-$ anion. While in the LHCE, the position and strength of the two peaks were not changed remarkably compared with the HCE. Meanwhile, the variation of the THF ring vibration peak could also prove the solvation structure of the HCE and LHCE. (Figure S6) Raman analysis results show that high salt concentration can reduce the free solvent molecules. The result above is proved in the characterization of ^{7}Li NMR, as shown in Figure 3h. The chemical shift moved to a higher field as salt increased, suggesting that more anions appeared around Li+. However, when HFE was added into the electrolyte, although the inner structure was not changed, the chemical shift moved to a lower field because HFE lay in the outer solvation structure and had

a shielding effect on Li+. This unique solvation structure of the HCE and LHCE could boost the antioxidation ability of the THF-based electrolyte, which is discussed in Figure S7.

The room-temperature electrochemical performance of Li/LMO cells with a voltage range from 3.0 to 4.2 V is demonstrated in Figure 4a. The cells in the 1m electrolyte displayed a sharp capacity decay at 120 cycles, maintaining only 74.5 mAh g^{-1} capacity for 200 cycles. (81.1%). As a comparison, the 5m and 5m-HFE41 electrolytes deliver capacities of 79.5 mAh g^{-1} (84.1%) and 81.6 mAh g^{-1} (85.9%) after 300 cycles, respectively (Figure 4b). Apart from that, the 5m-HFE41 electrolyte demonstrated better high-rate performance than 1m (50.0 mAh g^{-1}) and 5m electrolytes (59.7 mAh g^{-1}), maintaining 65.6 mAh g^{-1} (69.0%) capacity at the rate of 10C, as displayed in Figure 4c. Also, this electrolyte could cycle at a higher rate stably at room temperature (Figure S8). The improved rate performance of 5m-HFE41 can be ascribed to the following two reasons. First, although the conductivity of 5m-HFE41 is lower than other electrolytes at room temperature, its wettability with the separator is better, which ensures the bridging function of the electrolyte conducting ions between the cathode and anode. Second, 5m-HFE41 possesses a lower charge transfer activation energy and higher transference number, which facilitate the transportation of lithium ions in the interphase and bulk electrolyte (this will be discussed in the following part).

The morphology and chemical composition analysis of the lithium metal anode is displayed in Figure 5. The morphology of the 1m electrolyte is porous and uneven, while 5m and 5m-HFE41 are relatively dense and uniform, indicating that the side effect was inhibited in the HCE or LHCE (Figures 5a,4b,
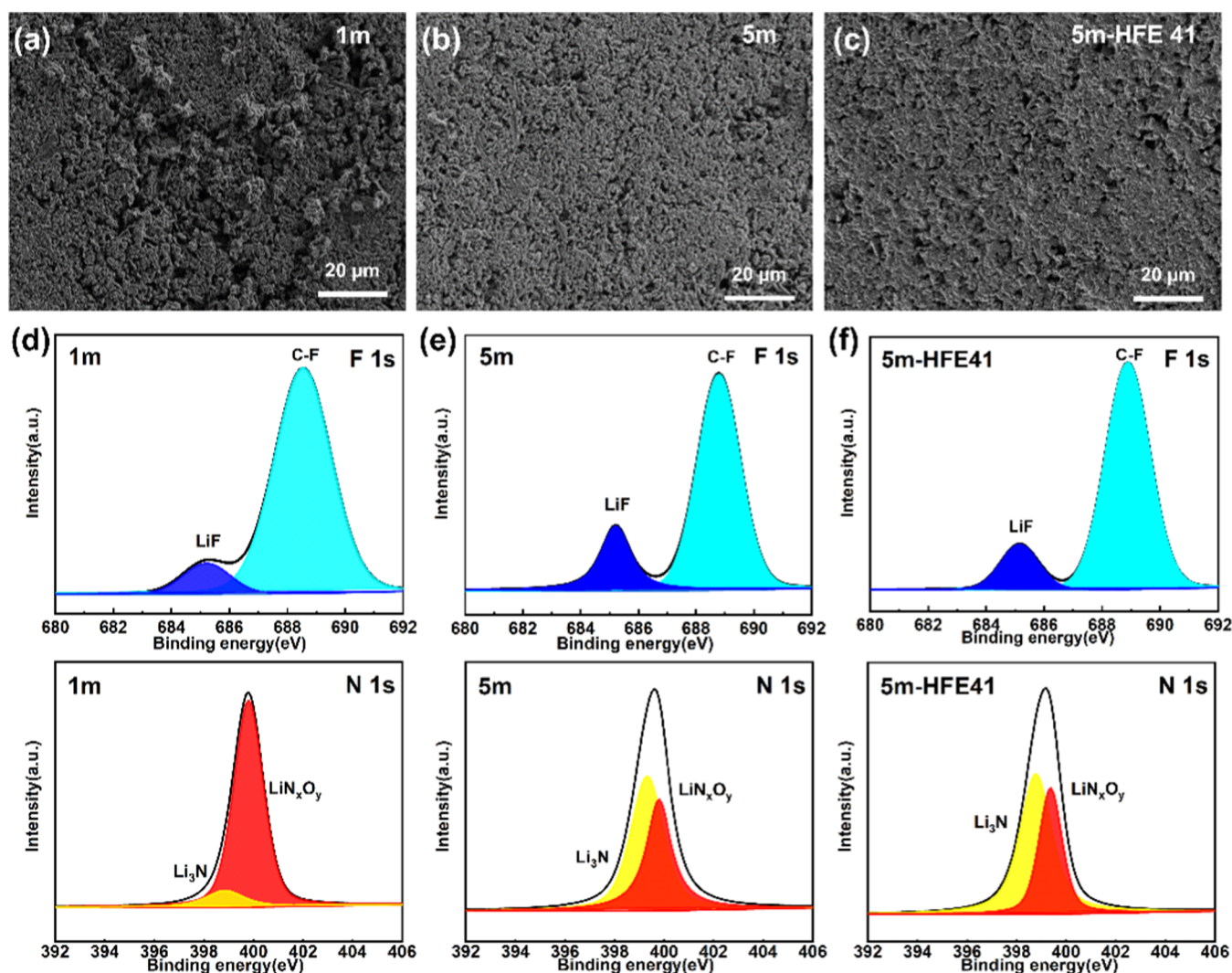
Figure 5. Morphology of lithium metal after 50 cycles in 1m (a), 5m (b), and 5m-HFE41(c) electrolytes. (d−f) XPS result of the lithium metal anode after 20 cycles in (d) 1m, (e) 5m, and (f) 5m-HFE41 electrolytes.

and 5c). The chemical components of the SEI in electrolytes are shown in Figure 5d−f. The component of LiF (684.8 eV) in 5m and 5m-HFE41 electrolytes is more obvious than that in the 1m electrolyte. On the other hand, the primary component of the SEI in these two electrolytes is Li_3N (398.3 eV), as demonstrated in the N 1s spectra. LiF and Li_3N are considered to provide sufficient mechanical strength and higher lithium-ion conductivity for the SEI in the previous literature.[45−47] The result of XPS can be attributed to the solvation structure of the HCE and LHCE, in which the anion tends to decompose into an inorganic component (e.g., LiF and Li_3N) when getting close to the surface of the anode (Figure S9).[48,49] These inorganic components not only conduct Li^+ but also isolate the transference of electrons, protecting lithium metal from a side reaction between the electrolyte and electrode. The Li/Cu cells in the HCE and LHCE demonstrated higher CE than in low-concentration electrolytes, as shown in Figure S10, suggesting the reversible stripping/deposition in the HCE and LHCE.

Apart from the anode, the interphase between the cathode and electrolyte also has a great impact on the cycling performance of Li/LMO cells. From the SEM result in Figure 6a−c, it can be seen that the particle of the 1m electrolyte was small and broken, indicating that the side reaction happened in the low-concentration electrolyte. Whereas in 5m and 5m-HFE41, the particle maintained a regular octahedral shape, which is nearly the same as the pristine sample (Figure S11). This result suggests that the latter two electrolytes could maintain the structural stability of LMO during cycling and thus ensure the stable cycling of the cell. The stability of the cathode structure is confirmed by the XRD test (Figure S12), in which the (111) and (311) peaks of the 1m electrolyte moved to a higher angle compared with the pristine sample, indicating a more severe shrinkage of the crystal lattice.[50] However, the 5m and 5m-HFE41 electrolytes showed lower angle variation, suggesting the structural stability of the LMO cathode. Figure 6d−f displays the elemental analysis of the LMO cathode, respectively. In the comparison of C 1s spectra, there are plenty of C−H and C−C bonds (284.4 eV, C 1s) and lithium carbonate (289.0 eV, C 1s) that exist on the LMO cathode surface in the 1m electrolyte, which is probably from the decomposition of the THF solvent. The decomposition product of the THF solvent is also detected in the O 1s spectra. Among the three electrolytes, the main component of the decomposition product in the 1m electrolyte includes lithium carbonate (532.4 eV, O 1s) and alkoxy lithium (531.4 eV, O 1s). Apart from that, transition metal ions may be
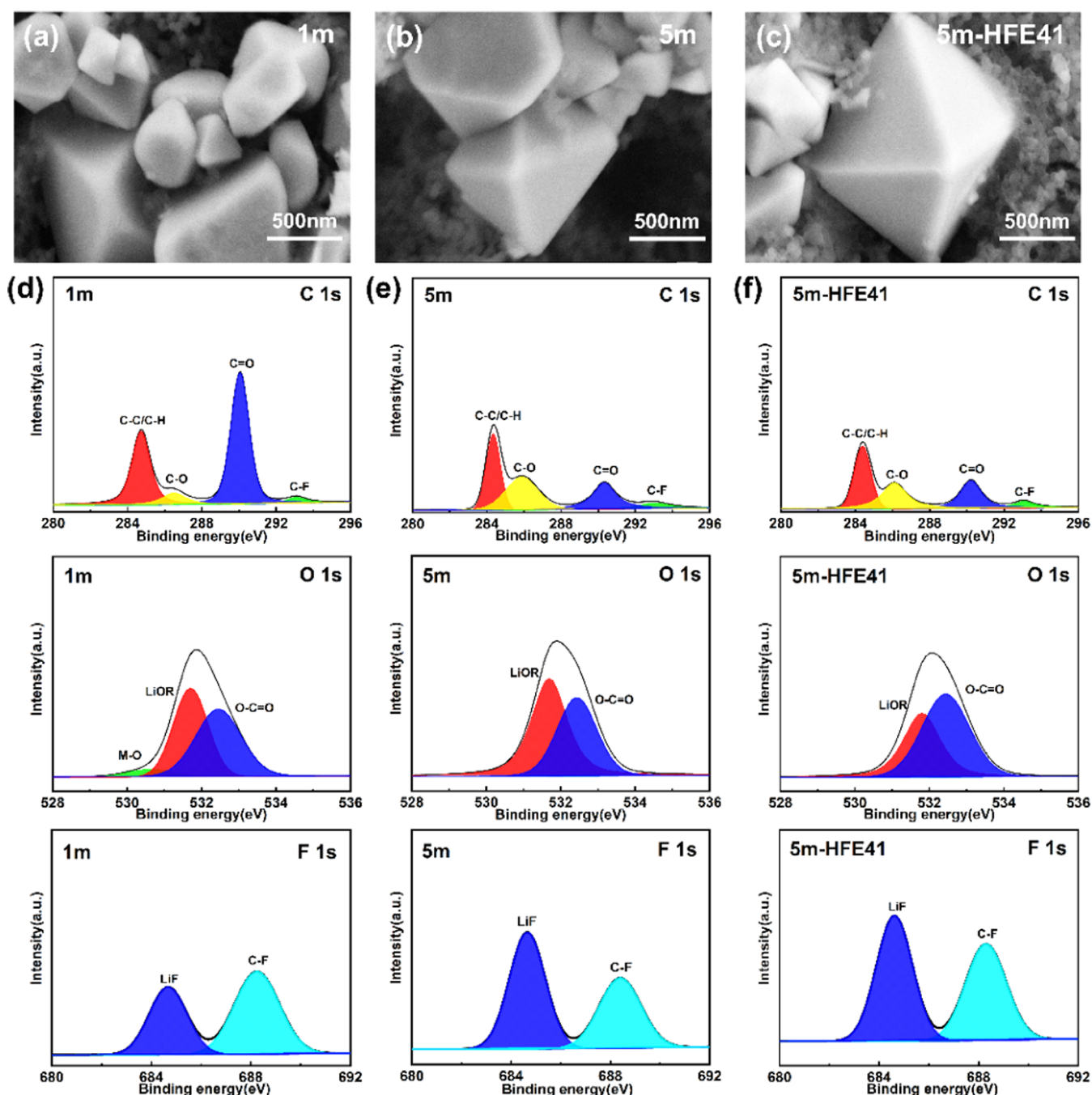
Figure 6. Morphology of the LMO cathode after 100 cycles in 1m (a), 5m (b), and 5m-HFE41(c) electrolytes. The chemical composition of the surface of the LMO cathode after 20 cycles in 1m (d), 5m (e), and 5m-HFE41 (f) electrolytes.

dissolved from the cathode into the electrolyte, as evidenced in the M−O signal (530.4 eV, O 1s) and the separator (Figure S13). Besides, the F 1s spectra result revealed that the main component of CEI in 5m and 5m-HFE41 is LiF, which is beneficial for the cells' cycling performance.

In terms of the low-temperature test, the discharge behavior of electrolytes at −70 °C is displayed in Figure 7a. Due to the high viscosity and slow lithium-ion diffusion, the 5m electrolyte hardly delivered a specific capacity (merely 1.6 mAh g^{-1}) at such a low temperature, while the 1m and 5m-HFE41 electrolytes could deliver 44.7 mAh g^{-1} and 68.9 mAh g^{-1}. This improved performance of the 5m-HFE41 electrolyte is owing to the lower viscosity and improved diffusion ability in

electrolytes. The diffusion behavior of Li$^+$ in the bulk electrolyte can be determined by monitoring the MSD (Figure S14, Table S2). At 25 °C, the Li$^+$ diffusion coefficient of the 1m electrolyte was dramatically higher than the other two electrolytes, but at −70 °C, the 5m-HFE41 electrolyte displayed a little higher diffusion coefficient than the low-concentration electrolyte (1.85×10^{-7} vs 1.72×10^{-7} cm^2 s^{-1}). Besides, this optimized electrolyte could discharge at a high rate at low temperatures, as shown in Figure 7b. At a lower rate, the Li/LMO cells with the 1m electrolyte could deliver 84.7 mAh g^{-1}, higher than other electrolytes. For this phenomenon, we guess that the determined factor at a low rate is related to the conductivity and wettability of the
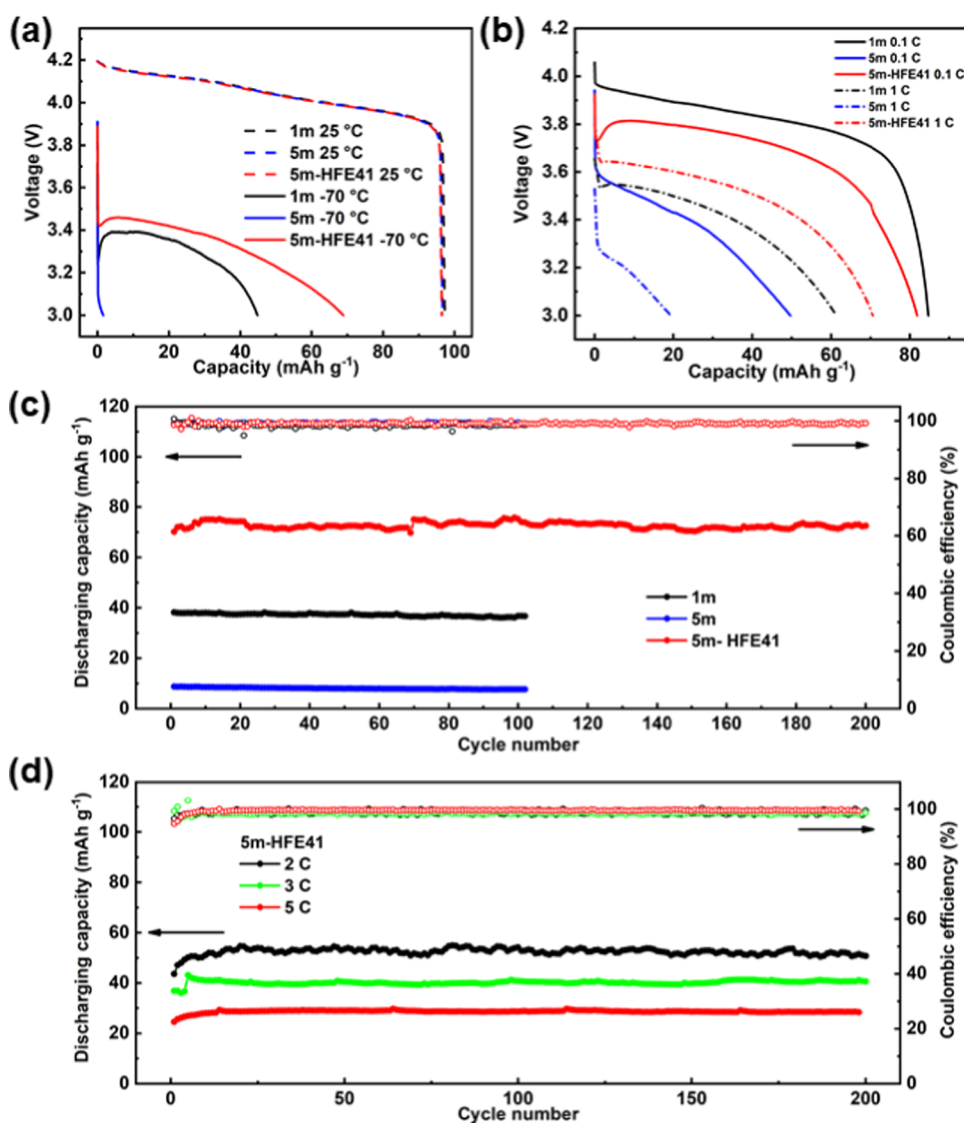
Figure 7. (a) Discharge performance of Li/LMO cells at 0.1C at −70 °C. (b) Discharge performance of Li/LMO cells at various rates at −40 °C. (c) Electrochemical performance of Li/LMO cells at a 1C rate at −40 °C. (d) Electrochemical performance of Li/LMO cells in the 5m-HFE41 electrolyte at a higher rate at −40 °C.

electrolyte. However, when the temperature was further decreased or the rate was further increased, the charge transfer became the key limiting factor. Therefore, when the rate increased to 1C, its specific capacity decreased to 61.4 mAh g^{-1}, lower than that of the 5m-HFE41 electrolyte. What is more, the 5m-HFE41 electrolyte could be discharged at a much higher rate (Figure S15). Apart from the discharge performance, the 5m-HFE41 electrolyte showed better cycling performance at 1C at −40 °C than other electrolytes, as shown in Figure 7c. The 5m electrolyte could hardly cycle due to its higher viscosity and slower lithium-ion diffusion at low temperatures, and the 1m electrolyte maintains only 36.7 mAh g^{-1} due to its poor kinetics at low temperatures. However, the 5m-HFE41 electrolyte has the both advantages of thermodynamics and kinetics, maintaining 77.1% capacity retention. What is more, the optimized electrolyte could even work at a higher rate, as demonstrated in Figure 7d. The remaining capacity of Li/LMO cells in the 5m-HFE41 electrolyte after 200 cycles is 50.7, 40.6, and 28.4 mAh g^{-1} at 2C, 3C, and 5C, respectively. All in all, the Li/LMO cells in

the optimized electrolyte demonstrate good low-temperature performance compared with other reported works (Table S4).

Figure 8a−c demonstrates the temperature-dependent EIS result of Li/LMO cells, which is used to calculate the corresponding activation energy. It is generally believed that the resistance of the battery can be divided into four parts according to the frequency (Figure 8d): bulk resistance (R_b, higher than 10^5 Hz), resistance of the SEI (R_{SEI}, from 10^5 to 10^3 Hz), charge transfer resistance (R_{ct}, from 10^3 to 10^0 Hz), and Warburg diffusion resistance (W, lower than 10^0 Hz).[51,52] Among them, the activation energy of R_{SEI} means the transportation of Li$^+$ through the SEI, while the activation energy of R_{ct} is related to the desolvation process of Li$^+$, which is regarded as the main reason determining the cells' low-temperature performance. The activation energy of R_{SEI} and R_{ct} is illustrated in Figure 8e,f, where the activation energy of the 5m-HFE41 electrolyte in any process is lower than that of 1m or 5m electrolytes, indicating fast lithium-ion transportation. The Tafel plot obtained from the Li/Li symmetric cell can provide another effective evidence for the kinetics of Li$^+$
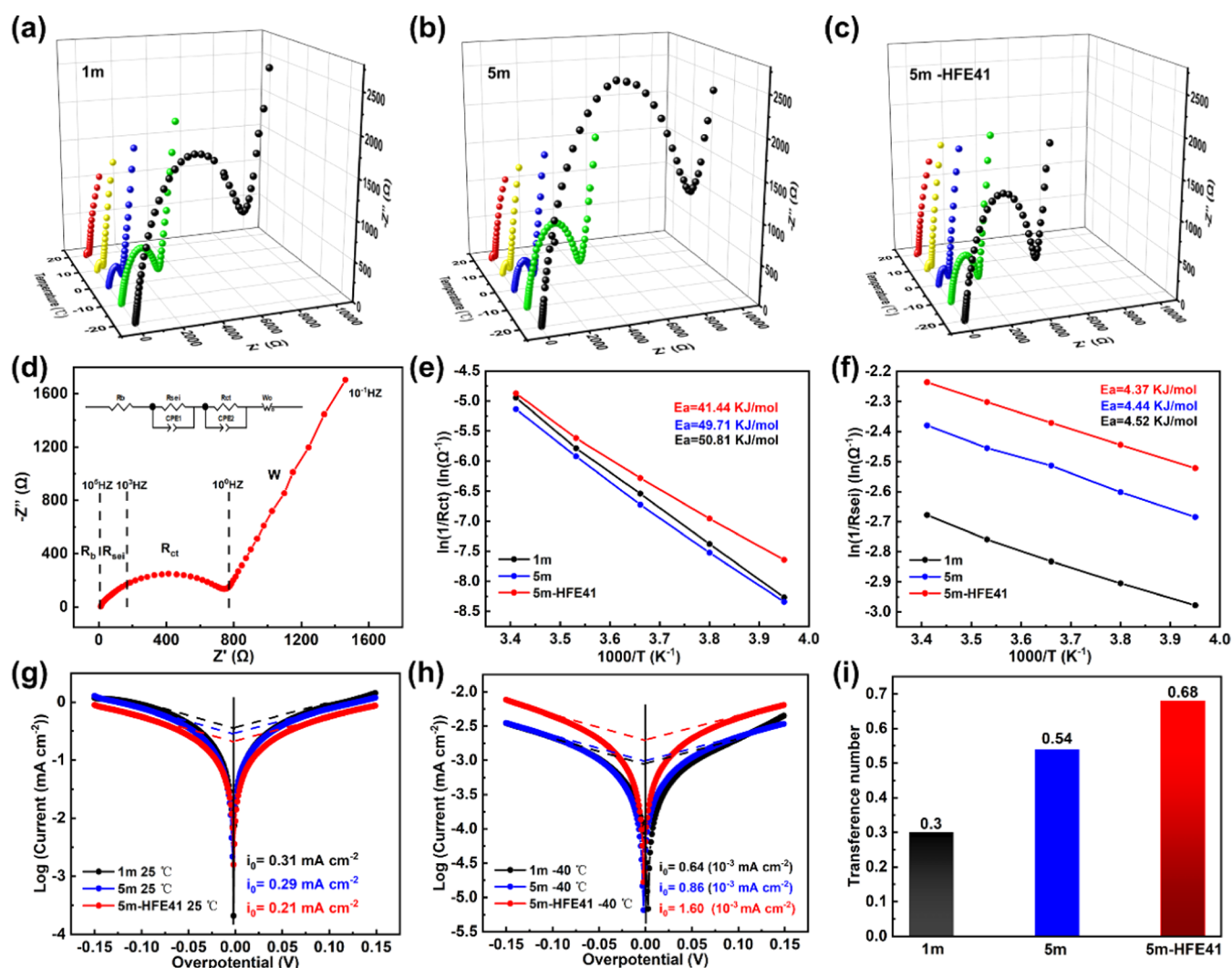
Figure 8. Analysis of kinetics. (a−c) Temperature-dependent EIS of Li/LMO cells at a fully discharged state in different electrolytes. (d) Schematic illustration of the equivalent circuit. The calculated activation energy of (e) R_{SEI} and (f) R_{ct}. The Tafel plot of Li/Li symmetric cells in three electrolytes at 25 °C (g) and at −40 °C (h). (i) Li$^+$ transference number (t_{Li^+}) of electrolytes.

transfer behavior. Figure 8g,h is the Tafel plot of the electrolytes at 25 and −40 °C, respectively. The 5m-HFE41 electrolyte, although the calculated exchange current density is lower than 1m at room temperature, exhibited much higher exchange current density (1.60×10^{-3} mA cm^{-2}) than 1m (0.64×10^{-3} mA cm^{-3}) and 5m (0.86×10^{-3} mA cm^{-3}) electrolytes at −40 °C. Also, the Li$^+$ transference number of 5m-HFE41 is 0.68, higher than those of 1m (0.3) and 5m (0.54) electrolytes (Figures 8i and S16). By the comparisons above, it can be found that the solvation structure rich in anions shows obvious kinetic advantages, especially at low temperatures. As for the 5m electrolyte, although this electrolyte possesses such a special solvation structure, the too high viscosity restricts its application in the low-temperature field. And such a restriction was lifted by adding the proper amount of diluent, which could facilitate the transference of Li$^+$ without giving away the advantage of the anion-rich solvated structure.

4. CONCLUSIONS

In conclusion, we design a THF-based localized high-concentration electrolyte. This electrolyte possessed higher

conductivity and lower viscosity than high-concentration electrolytes at low temperatures, which facilitates the diffusion of lithium ions in a cryogenic environment. The MD and spectral analyses were conducted to confirm the anion-dominate solvation structure of the HCE and LHCE, which promoted the desolvation process of lithium ions at the interphase and thus guaranteed excellent high-rate and low-temperature performance. Because of their unique solvation structure, the SEI and CEI full of inorganic components were formed at the surface of the anode and cathode, respectively, which inhibited the side reaction at the electrolyte/electrode interface. Li/LMO with the optimized electrolyte maintained 85.9% capacity retention at room temperature and it could be worked at a 10C rate with 69.0% capacity retention. Apart from that, it can enable Li/LMO cells to discharge at −70 °C and to maintain 72.5 mAh g^{-1} capacity for 200 cycles. And it also can cycle even though the rate was raised to 5C, showing excellent cycling performance. It is universally established that the HCE is a sound strategy to form a favorable solvation structure involving more anions in the primary solvation sheath. And adding a proper amount of diluent into the HCE could expand its application at low temperatures by reducing

the viscosity without altering the solvation structure significantly. It is the combination of the better mobility of low concentration and the unique solvation behavior of high concentration that enables the fast kinetics of Li/LMO cells, as manifested in the EIS, Tafel, and Li$^+$ transference number tests. All in all, this work shows that the LHCE is capable of low temperature and fast kinetics, providing a reference for the low-temperature electrolyte design.

■ ASSOCIATED CONTENT

ⓢ Supporting Information

The Supporting Information is available free of charge at https://pubs.acs.org/doi/10.1021/acsami.3c04747.

> Conductivity and viscosity test; contact angle test; MD simulation; Raman test; DFT calculation; LSV test; cycling performance of Li/LMO at a higher rate; Li/Cu cell test; SEM of pristine LMO; XRD results; EDS mapping; MSD result; discharge performance of Li/LMO at −40 °C at a higher rate; and Li$^+$ transference number (PDF)

■ AUTHOR INFORMATION

Corresponding Authors

Peng Zhang − *College of Energy, Xiamen University, Xiamen 361102, P. R. China*; Email: pengzhang@xmu.edu.cn

Jinbao Zhao − *State-Province Joint Engineering Laboratory of Power Source Technology for New Energy Vehicle, Engineering Research Center of Electrochemical Technology, Ministry of Education, College of Chemistry and Chemical Engineering, Xiamen University, Xiamen 361005, P. R. China; College of Energy, Xiamen University, Xiamen 361102, P. R. China;* ⓞ orcid.org/0000-0002-2753-7508; Phone: +86-05922186935; Email: jbzhao@xmu.edu.cn

Authors

Pengbin Lai − *State-Province Joint Engineering Laboratory of Power Source Technology for New Energy Vehicle, Engineering Research Center of Electrochemical Technology, Ministry of Education, College of Chemistry and Chemical Engineering, Xiamen University, Xiamen 361005, P. R. China*

Xiaodie Deng − *State-Province Joint Engineering Laboratory of Power Source Technology for New Energy Vehicle, Engineering Research Center of Electrochemical Technology, Ministry of Education, College of Chemistry and Chemical Engineering, Xiamen University, Xiamen 361005, P. R. China*

Yaqi Zhang − *State-Province Joint Engineering Laboratory of Power Source Technology for New Energy Vehicle, Engineering Research Center of Electrochemical Technology, Ministry of Education, College of Chemistry and Chemical Engineering, Xiamen University, Xiamen 361005, P. R. China*

Jialin Li − *State-Province Joint Engineering Laboratory of Power Source Technology for New Energy Vehicle, Engineering Research Center of Electrochemical Technology, Ministry of Education, College of Chemistry and Chemical Engineering, Xiamen University, Xiamen 361005, P. R. China*

Haiming Hua − *State-Province Joint Engineering Laboratory of Power Source Technology for New Energy Vehicle, Engineering Research Center of Electrochemical Technology,*

Ministry of Education, College of Chemistry and Chemical Engineering, Xiamen University, Xiamen 361005, P. R. China

Boyang Huang − *State-Province Joint Engineering Laboratory of Power Source Technology for New Energy Vehicle, Engineering Research Center of Electrochemical Technology, Ministry of Education, College of Chemistry and Chemical Engineering, Xiamen University, Xiamen 361005, P. R. China*

Complete contact information is available at: https://pubs.acs.org/10.1021/acsami.3c04747

Notes

The authors declare no competing financial interest.

■ ACKNOWLEDGMENTS

■ REFERENCES

(1) Huang, C.-K.; Sakamoto, J. S.; Wolfenstine, J.; Surampudi, S. The Limits of Low-Temperature Performance of Li-Ion Cells. *J. Electrochem. Soc* **2000**, *147*, 2893−2896.

(2) Li, Q.; Jiao, S.; Luo, L.; Ding, M. S.; Zheng, J.; Cartmell, S. S.; Wang, C.-M.; Xu, K.; Zhang, J.-G.; Xu, W. Wide-Temperature Electrolytes for Lithium-Ion Batteries. *ACS Appl. Mater. Interfaces* **2017**, *9*, 18826−18835.

(3) Hou, J.; Yang, M.; Wang, D.; Zhang, J. Fundamentals and Challenges of Lithium Ion Batteries at Temperatures between −40 and 60 °C. *Adv. Energy Mater.* **2020**, *10*, No. 1904152.

(4) Zhang, S. S.; Xu, K.; Jow, T. R. The low temperature performance of Li-ion batteries. *J. Power Sources* **2003**, *115*, 137−140.

(5) Zhang, J.; Zhang, J.; Liu, T.; Wu, H.; Tian, S.; Zhou, L.; Zhang, B.; Cui, G. Toward Low-Temperature Lithium Batteries: Advances and Prospects of Unconventional Electrolytes. *Adv. Energy Sustainability Res.* **2021**, *2*, No. 2100039.

(6) Liu, J.; Bao, Z.; Cui, Y.; Dufek, E. J.; Goodenough, J. B.; Khalifah, P.; Li, Q.; Liaw, B. Y.; Liu, P.; Manthiram, A.; Meng, Y. S.; Subramanian, V. R.; Toney, M. F.; Viswanathan, V. V.; Whittingham, M. S.; Xiao, J.; Xu, W.; Yang, J.; Yang, X.-Q.; Zhang, J.-G. Pathways for practical high-energy long-cycling lithium metal batteries. *Nat. Energy* **2019**, *4*, 180−186.

(7) Thenuwara, A. C.; Shetty, P. P.; McDowell, M. T. Distinct Nanoscale Interphases and Morphology of Lithium Metal Electrodes Operating at Low Temperatures. *Nano Lett.* **2019**, *19*, 8664−8672.

(8) Ren, X.; Zou, L.; Cao, X.; Engelhard, M. H.; Liu, W.; Burton, S. D.; Lee, H.; Niu, C.; Matthews, B. E.; Zhu, Z.; Wang, C.; Arey, B. W.; Xiao, J.; Liu, J.; Zhang, J.-G.; Xu, W. Enabling High-Voltage Lithium-Metal Batteries under Practical Conditions. *Joule* **2019**, *3*, 1662−1676.

(9) Xu, W.; Wang, J.; Ding, F.; Chen, X.; Nasybulin, E.; Zhang, Y.; Zhang, J.-G. Lithium metal anodes for rechargeable batteries. *Energy Environ. Sci.* **2014**, *7*, 513−537.

(10) Zhang, N.; Deng, T.; Zhang, S.; Wang, C.; Chen, L.; Wang, C.; Fan, X. Critical review on low-temperature Li-ion/metal batteries. *Adv. Mater.* **2021**, No. e2107899.

(11) Collins, G. A.; Geaney, H.; Ryan, K. M. Alternative anodes for low temperature lithium-ion batteries. *J. Mater. Chem. A* **2021**, *9*, 14172−14213.

(12) Rodrigues, M.-T. F.; Babu, G.; Gullapalli, H.; Kalaga, K.; Sayed, F. N.; Kato, K.; Joyner, J.; Ajayan, P. M. A materials perspective on Li-ion batteries at extreme temperatures. *Nat. Energy* **2017**, *2*, No. 17108.

(13) Zhou, Z.; Li, G.; Zhang, J.; Zhao, Y. Wide Working Temperature Range Rechargeable Lithium−Sulfur Batteries: A Critical Review. *Adv. Funct. Mater.* **2021**, DOI: 10.1002/adfm.202107136.

(14) Yue-ru, G. U.; Wei-min, Z.; Chang-hu, S. U.; Chuan-jun, L. U. O.; Zhong-ru, Z.G.; Xu-jin, X. U. E.; Yong, Y. Research Progresses in Improvement for Low Temperature Performance of Lithium-Ion Batteries. *J. Electroanal. Chem.* **2018**, *24*, 488−496.

(15) Kim, N.; Myung, Y.; Kang, H.; Lee, J. W.; Yang, M. Effects of Methyl Acetate as a Co-Solvent in Carbonate-Based Electrolytes for Improved Lithium Metal Batteries. *ACS Appl. Mater. Interfaces* **2019**, *11*, 33844−33849.

(16) Cai, G.; Holoubek, J.; Xia, D.; Li, M.; Yin, Y.; Xing, X.; Liu, P.; Chen, Z. An ester electrolyte for lithium-sulfur batteries capable of ultra-low temperature cycling. *Chem. Commun.* **2020**, *56*, 9114−9117.

(17) Xu, J.; Wang, X.; Yuan, N.; Ding, J.; Qin, S.; Razal, J. M.; Wang, X.; Ge, S.; Gogotsi, Y. Extending the low temperature operational limit of Li-ion battery to −80 °C. *Energy Storage Mater.* **2019**, *23*, 383−389.

(18) Thenuwara, A. C.; Shetty, P. P.; Kondekar, N.; Sandoval, S. E.; Cavallaro, K.; May, R.; Yang, C.-T.; Marbella, L. E.; Qi, Y.; McDowell, M. T. Efficient Low-Temperature Cycling of Lithium Metal Anodes by Tailoring the Solid-Electrolyte Interphase. *ACS Energy Lett.* **2020**, *5*, 2411−2420.

(19) Cho, Y.-G.; Kim, Y.-S.; Sung, D.-G.; Seo, M.-S.; Song, H.-K. Nitrile-assistant eutectic electrolytes for cryogenic operation of lithium ion batteries at fast charges and discharges. *Energy Environ. Sci.* **2014**, *7*, 1737−1743.

(20) Zhao, Q.; Zhang, Y.; Tang, F.; Zhao, J.; Li, S. Mixed Salts of Lithium Difluoro (Oxalate) Borate and Lithium Tetrafluorobotate Electrolyte on Low-Temperature Performance for Lithium-Ion Batteries. *J. Electrochem. Soc* **2017**, *164*, A1873−A1880.

(21) Li, Q.; Lu, D.; Zheng, J.; Jiao, S.; Luo, L.; Wang, C. M.; Xu, K.; Zhang, J. G.; Xu, W. Li +-Desolvation Dictating Lithium-Ion Battery's Low-Temperature Performances. *ACS Appl. Mater. Interfaces* **2017**, *9*, 42761−42768.

(22) Zhang, S. S.; Xu, K.; Jow, T. R. Electrochemical impedance study on the low temperature of Li-ion batteries. *Electrochim. Acta* **2004**, *49*, 1057−1061.

(23) Holoubek, J.; Liu, H.; Wu, Z.; Yin, Y.; Xing, X.; Cai, G.; Yu, S.; Zhou, H.; Pascal, T. A.; Chen, Z.; Liu, P. Tailoring Electrolyte Solvation for Li Metal Batteries Cycled at Ultra-Low Temperature. *Nat. Energy* **2021**, *6*, 303−313.

(24) Fan, X.; Ji, X.; Chen, L.; Chen, J.; Deng, T.; Han, F.; Yue, J.; Piao, N.; Wang, R.; Zhou, X.; Xiao, X.; Chen, L.; Wang, C. All-temperature batteries enabled by fluorinated electrolytes with non-polar solvents. *Nat. Energy* **2019**, *4*, 882−890.

(25) Shi, J.; Xu, C.; Lai, J.; Li, Z.; Zhang, Y.; Liu, Y.; Ding, K.; Cai, Y.-P.; Shang, R.; Zheng, Q. An Amphiphilic Molecule-Regulated Core-Shell-Solvation Electrolyte for Li-Metal Batteries at Ultra-Low Temperature. *Angew. Chem., Int. Ed.* **2023**, *62*, No. e202218151.

(26) Li, Z.; Rao, H.; Atwi, R.; Sivakumar, B. M.; Gwalani, B.; Gray, S.; Han, K. S.; Everett, T. A.; Ajantiwalay, T. A.; Murugesan, V.; Rajput, N. N.; Pol, V. G. Non-polar ether-based electrolyte solutions for stable high-voltage non-aqueous lithium metal batteries. *Nat. Commun.* **2023**, *14*, No. 868.

(27) Zhang, G.; Chang, J.; Wang, L.; Li, J.; Wang, C.; Wang, R.; Shi, G.; Yu, K.; Huang, W.; Zheng, H.; Wu, T.; Deng, Y.; Lu, J. A monofluoride ether-based electrolyte solution for fast-charging and low-temperature non-aqueous lithium metal batteries. *Nat. Commun.* **2023**, *14*, No. 1081.

(28) Zhang, H.; Zeng, Z.; Ma, F.; Wu, Q.; Wang, X.; Cheng, S.; Xie, J. Cyclopentylmethyl Ether, a Non-Fluorinated, Weakly Solvating and Wide Temperature Solvent for High-Performance Lithium Metal Battery. *Angew. Chem., Int. Ed.* **2023**, No. e202300771.

(29) Holoubek, J.; Kim, K.; Yin, Y.; Wu, Z.; Liu, H.; Li, M.; Chen, A.; Gao, H.; Cai, G.; Pascal, T. A.; Liu, P.; Chen, Z. Electrolyte design implications of ion-pairing in low-temperature Li metal batteries. *Energy Environ. Sci.* **2022**, *15*, 1647−1658.

(30) Dong, X.; Lin, Y.; Li, P.; Ma, Y.; Huang, J.; Bin, D.; Wang, Y.; Qi, Y.; Xia, Y. High-Energy Rechargeable Metallic Lithium Battery at −70 degrees C Enabled by a Cosolvent Electrolyte. *Angew. Chem., Int. Ed.* **2019**, *58*, 5623−5627.

(31) Lai, P.; Huang, B.; Deng, X.; Li, J.; Hua, H.; Zhang, P.; Zhao, J. A localized high concentration carboxylic ester-based electrolyte for high-voltage and low temperature lithium batteries. *Chem. Eng. J.* **2023**, *461*, No. 141904.

(32) Pham, T. D.; Bin Faheem, A.; Lee, K. K. Design of a LiF-Rich Solid Electrolyte Interphase Layer through Highly Concentrated LiFSI-THF Electrolyte for Stable Lithium Metal Batteries. *Small* **2021**, *17*, No. e2103375.

(33) Frisch, M. J.; Trucks, G. W.; Fox, D. J. et al. *Gaussian 09*, revision E. 01; Gaussian, Inc.: Wallingford CT, 2013.

(34) Stephens, P. J.; Devlin, F. J.; Chabalowsk, C. F.; Frisch, M. J. Ab Initio Calculation of Vibrational Absorption and Circular Dichroism Spectra Using Density Functional Force Fields. *J. Phys. Chem. A* **1994**, *98*, 11623−11627.

(35) Grimme, S.; Antony, J.; Ehrlich, S.; Krieg, H. A consistent and accurate ab initio parametrization of density functional dispersion correction (DFT-D) for the 94 elements H-Pu. *J. Chem. Phys.* **2010**, *132*, No. 154104.

(36) Krishnan, R.; Binkley, J. S.; Seeger, R.; Pople, J. A. Self-consistent molecular orbital methods. XX. A basis set for correlated wave functions. *J. Chem. Phys.* **1980**, *72*, 650−654.

(37) Clark, T.; Jayaraman, C.; Spitznagel, G. W.; Schleyer, P. V. R. Efficient Diffuse Function- Augmented Basis Sets for Anion Calculations. III.* The 3-21 + G Basis Set for First-Row Elements, Li-F. *J. Comput. Chem.* **1983**, *4*, 294−301.

(38) Sun, H. COMPASS: An ab Initio Force-Field Optimized for Condensed-Phase ApplicationssOverview with Details on Alkane and Benzene Compounds. *J. Phys. Chem. B 102* 7338 7364. DOI: 10.1021/jp980939v.

(39) Essmann, U.; Lalith, P.; Berkowitz, M. L.; et al. A smooth particle mesh Ewald method. *J. Chem. Phys.* **1995**, *103*, 8577−8593.

(40) Lai, P.; Hua, H.; Huang, B.; Zhang, P.; Zhao, J. A Carboxylic Ester-Based Electrolyte with Additive to Improve Performance of Lithium Batteries at Ultra-Low Temperature. *J. Electrochem. Soc.* **2022**, *169*, No. 100539.

(41) Adams, B. D.; Zheng, J.; Ren, X.; Xu, W.; Zhang, J. G. Accurate Determination of Coulombic Efficiency for Lithium Metal Anodes and Lithium Metal Batteries. *Adv. Energy Mater.* **2017**, *8*, No. 1702097.

(42) Yamada, Y.; Furukawa, K.; Sodeyama, K.; Kikuchi, K.; Yaegashi, M.; Tateyama, Y.; Yamada, A. Unusual stability of acetonitrile-based superconcentrated electrolytes for fast-charging lithium-ion batteries. *J. Am. Chem. Soc.* **2014**, *136*, 5039−46.

(43) Yamada, Y.; Wang, J.; Ko, S.; Watanabe, E.; Yamada, A. Advances and issues in developing salt-concentrated battery electrolytes. *Nat. Energy* **2019**, *4*, 269−280.

(44) Mandal, B. K.; Padhi, A. K.; Shi, Z.; Chakraborty, S.; Filler, R. LiTFSI New low temperature electrolytes with thermal runaway inhibition for lithium-ion rechargeable batteries. *J. Power Source* **2006**, *162*, 690−695.

(45) Lu, Y.; Tu, Z.; Archer, L. A. Stable lithium electrodeposition in liquid and nanoporous solid electrolytes. *Nat. Mater.* **2014**, *13*, 961−969.

(46) Shi, K.; Wan, Z.; Yang, L.; Zhang, Y.; Huang, Y.; Su, S.; Xia, H.; Jiang, K.; Shen, L.; Hu, Y.; Zhang, S.; Yu, J.; Ren, F.; He, Y. B.; Kang, F. In Situ Construction of an Ultra-Stable Conductive Composite

Interface for High-Voltage All-Solid-State Lithium Metal Batteries. *Angew. Chem., Int. Ed.* **2020**, *59*, 11784−11788.

(47) Yu, J.; Shi, K.; Zhang, S.; Zhang, D.; Chen, L.; Li, S.; Ma, J.; Xia, H.; He, Y.-B. A lithium nucleation-diffusion-growth mechanism to govern the horizontal deposition of lithium metal anode. *Sci. China Mater.* **2021**, *64*, 2409−2420.

(48) Eshetu, G. G.; Judez, X.; Li, C.; Martinez-Ibanez, M.; Gracia, I.; Bondarchuk, O.; Carrasco, J.; Rodriguez-Martinez, L. M.; Zhang, H.; Armand, M. Ultrahigh Performance All Solid-State Lithium Sulfur Batteries: Salt Anion's Chemistry-Induced Anomalous Synergistic Effect. *J. Am. Chem. Soc.* **2018**, *140*, 9921−9933.

(49) Hou, L. P.; Zhang, X. Q.; Li, B. Q.; Zhang, Q. Cycling a Lithium Metal Anode at 90 degrees C in a Liquid Electrolyte. *Angew. Chem., Int. Ed.* **2020**, *59*, 15109−15113.

(50) Li, B.; Wang, Y.; Rong, H.; Wang, Y.; Liu, J.; Xing, L.; Xu, M.; Li, W. A novel electrolyte with the ability to form a solid electrolyte interface on the anode and cathode of a LiMn2O4/graphite battery. *J. Mater. Chem. A* **2013**, *1*, 12954−12961.

(51) Zheng, X.; Gu, Z.; Fu, J.; Wang, H.; Ye, X.; Huang, L.; Liu, X.; Wu, X.; Luo, W.; Huang, Y. Knocking down the kinetic barriers towards fast-charging and low-temperature sodium metal batteries. *Energy Environ. Sci.* **2021**, *14*, 4936−4947.

(52) Fang, Z.; Yang, Y.; Zheng, T.; Wang, N.; Wang, C.; Dong, X.; Wang, Y.; Xia, Y. An all-climate CFx/Li battery with mechanism-guided electrolyte. *Energy Storage Mater.* **2021**, *42*, 477−483.